A Fractional Calculus Model of Viscoelastic Stator Supports Coupled With Elastic Rotor–Stator Rub

Patrick A. Smyth
Georgia Institute of Technology,
School of Mechanical Engineering,
Atlanta, GA 30332
e-mail: pasmyth4@gatech.edu

Philip A. Varney
Georgia Institute of Technology,
School of Mechanical Engineering,
Atlanta, GA 30332
e-mail: pvarney3@gatech.edu

Itzhak Green
Georgia Institute of Technology,
School of Mechanical Engineering,
Atlanta, GA 30332
e-mail: itzhak.green@me.gatech.edu

Rotating machinery is inherently susceptible to costly and dangerous faults. One such commonly encountered fault is undesirable dynamic contact between the rotor and stator (i.e., rotor–stator rub). The forces generated during rotor–stator rub are fundamentally tribological, as they are generated by contact and friction and result in wear. These forces are typically found by assuming linear elastic contact and dry Coulomb friction at the rotor–stator interface, where the normal force is a linear function of the interference. For the first time, this work incorporates viscoelasticity into the stator support and investigates its influence on the global dynamics of rotor–stator rub. The viscoelastic stator supports are modeled using fractional calculus, an approach which adeptly and robustly characterizes the viscoelasticity. Specifically, a fractional derivative order of one-half is employed to generate an analytic time-domain form of viscoelastic impedance. This approach directly assimilates viscoelasticity into the system dynamics, since the rotor equations of motion are integrated numerically in the time-domain. The coupled rotor–stator dynamic model incorporating viscoelastic supports is solved numerically to explore the influence of viscoelasticity. This model provides a framework for analysis of dynamic systems where viscoelasticity is included. [DOI: 10.1115/1.4032787]

1 Introduction

Fluid film triboelements are an integral component of many rotating machines; unfortunately, finite clearances within these components are susceptible to rotor–stator contact (i.e., rub) [1]. Rotor–stator rub is an undesirable phenomenon that results in detrimental machine operation via increased wear, vibration, and thermal stresses, which in turn contribute to reduced component life. Although contact is an undesirable mode of operation, it is often unavoidable in rotating machines. When contact occurs, large impulsive forces can quickly damage machine components prior to detection via condition monitoring. Thus, methods should be sought to minimize adverse contact effects, either by changing the operating conditions, or by distributing contact forces to reduce damage and wear. To explore these concepts, proper modeling of system components and physics is required.

A brief treatise on rotor–stator rub is provided prior to surveying works including rotor viscoelasticity. Rotor–stator rub systems are piecewise-smooth hybrid dynamic systems [2], and consequentially, result in incredibly rich nonlinear dynamics, including periodic, quasiperiodic, and chaotic responses [3–6]. Furthermore, a diverse array of bifurcations is observed as routes to chaos, including period doubling, quasiperiodic routes, intermittency, and grazing. These bifurcations are also observed for other control parameters, including, for example, shaft speed, external viscous damping, eccentricity, and clearance. Therefore, investigating rotor–stator rub systems requires carefully controlling all parameters of interest, as even small deviations can result in dramatic changes in the rotor response. It is also important to note that this introduction does not serve as a treatise on all rotor–stator rub investigations; such information is available in other works [4,7,8].

Rotor–stator rub is typically classified according to its extent: partial rub or full rub. Partial rubs occur intermittently, and do not usually threaten the machine. Even though partial rubs are not typically dangerous, they may be symptomatic of other component failures. Partial rub is worthwhile to investigate in order to detect and mitigate rub prior to more severe full rub conditions. Full rub conditions occur when the rotor maintains constant contact with the stator and processes in either a forward or backward motion [9–11]. The backward whirl case represents the greater threat, and is classified as either dry-friction backward whirl, where the rotor rolls without slip along the stator, or dry-friction backward whip, where the rotor slips along the stator in a direction opposite shaft rotation. These phenomena occur under specific operating conditions and parameter regimes, and do not constitute the majority of rub occurrences. As such, this work does not seek to address these phenomena.

Several other works have considered the use of viscoelastic components in rotor systems experiencing rub. Cao et al. [12] incorporated a fractional-order damping model (i.e., viscoelasticity) into a rub-impact rotor system, where viscoelasticity is included by replacing the external viscous damping force with a fractional calculus damping element. Their work concludes that such a modification results in chaotic, quasiperiodic, and periodic motions; however, these same responses are also encountered when only simple viscous damping models are used [4,5]. Though their work is useful conceptually, much work remains toward understanding rotordynamics coupled with viscoelasticity. Patel et al. [13] investigated a viscoelastically supported stator experiencing rub, though they consider a stator support which constitutes only a linear spring and viscous damper in parallel; this representation does not truly represent viscoelasticity.

Though the study of viscoelasticity in rotor contact is limited in scope, more authors have generally considered viscoelastic supports in noncontacting rotor-bearing systems. Dutt and Nakra [14] demonstrated that including viscoelasticity in the rotor supports results in an increased regime of stability. Lee et al. [15] developed a viscoelastic foil bearing, where the bearing's increased viscous damping results in a reduction in vibration magnitude near the bending critical speed when compared to a more conventional bump foil bearing. Shabaneh and Zu [16] studied the influence of

Contributed by the Tribology Division of ASME for publication in the JOURNAL OF TRIBOLOGY. Manuscript received June 8, 2015; final manuscript received November 7, 2015; published online June 21, 2016. Assoc. Editor: Bugra Ertas.

viscoelastically suspended bearings on the critical speeds of a simple rotor, where the viscoelasticity is modeled using a Kelvin–Voigt element. Their results indicate that viscoelastically suspending the bearings results in significant changes in the rotor critical speeds.

In most cases, rotor–stator contact is not a normal operating condition, and usually is indicative of machine failure. A particular case where such a condition may occur is a rotor supported by active magnetic bearings (AMBs), where catcher bearings are employed to support the rotor in the event of AMB failure [17,18]. These catcher bearings are essentially specialized stators; therefore, their behavior can perhaps be better understood by including viscoelastic supports in rotordynamic simulations. This work will propose such a method for incorporating viscoelasticity into rotordynamic simulation.

Many viscoelastic models are comprised of spring and dashpot hierarchies; therefore, their inclusion in dynamic systems is natural. Any number of these spring and dashpot hierarchies exist with each model having time and strain-rate dependency. This translates to stress (and analogously, restoring force) being time and rate dependent. Many realistic support materials are viscoelastic (polymers), or effectively viscoelastic (squeeze-film bearings), so the inclusion of viscoelastic supports is appropriate in rotating systems. Constitutive viscoelastic models will be discussed herein.

A viscoelastically suspended stator will be included in a rotor–stator contact model. A Jeffcott rotor is employed as a conceptual test platform, using the common linear elastic contact model (LECM) originally developed by Beatty [19] and implemented by numerous other researchers. Because of its simplicity, the Jeffcott rotor model allows complex interactions between the contact phenomena and viscoelastic supports to be isolated and investigated. The viscoelasticity is captured in the support using a fractional-calculus representation. Rotor responses with and without viscoelasticity are provided as a comparison point for the model. Various responses will be shown for different property sets, indicating rich dynamic behavior of the system.

2 Modeling

Here, a dynamic model (i.e., equations of motion) for the viscoelastically suspended rotor–stator system will be presented. A Jeffcott rotor with cylindrical modes is used along with the LECM, where contact forces couple the rotor motion to that of the viscoelastically suspended stator. A method for incorporating a fractional-calculus representation of viscoelasticity into the stator support is also discussed herein.

2.1 Dynamics. The Jeffcott rotor and viscoelastically suspended stator are shown in Figs. 1 and 2, respectively, where $x_r y_r$ and $x_s y_s$ are translating inertial rotor and stator reference frames, respectively. The coupled system is represented in Fig. 3, and the

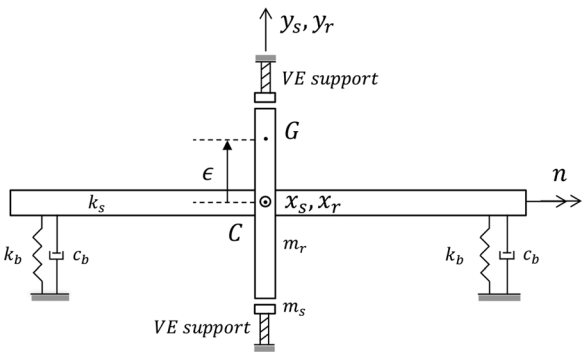

Fig. 1 Jeffcott rotor with corresponding viscoelastically suspended stator

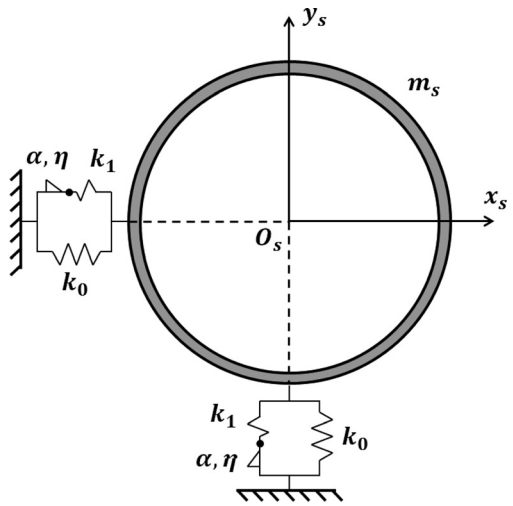

Fig. 2 Viscoelastically suspended stator

relationship between rotor and stator frames is vectorially illustrated in Fig. 4, where the rotor and stator degrees-of-freedom are their absolute inertial displacements from O (here, XY denotes an inertial frame fixed to the undeflected rotor/stator position, O). The system comprises four degrees-of-freedom: two orthogonal displacements for each component of interest, such that the absolute rotor and stator radial deflections are

$$\bar{r}_s = u_{xs}\hat{i} + u_{ys}\hat{j} \tag{1}$$

$$\bar{r}_r = u_{xr}\hat{i} + u_{yr}\hat{j} \tag{2}$$

The rotor's deflection relative to the stator is given by

$$\bar{r}_{r/s} = \bar{r}_r - \bar{r}_s = (u_{xr} - u_{xs})\hat{i} + (u_{yr} - u_{ys})\hat{j} \tag{3}$$

For brevity, the magnitude of the relative radial deflection will be denoted by $||\bar{r}_{r/s}|| = r'$. Thus, contact occurs when the rotor's relative deflection r' exceeds the clearance δ; once the clearance is exceeded, a normal restoring force $\bar{F}_c$ and tangential friction force $\bar{F}_f$ are generated at the contact interface (see Ref. [4] for details). Here, the LECM is used to calculate the contact forces. The normal restoring force $\bar{F}_c$ is proportional to the rotor–stator interference $r' - \delta$ by the contact stiffness k_c and occurs in a direction colinear but opposite to $\bar{r}_{r/s}$ (i.e., $-\hat{e}_{r'}$). Furthermore, this work considers only Coulomb friction, where the friction force is

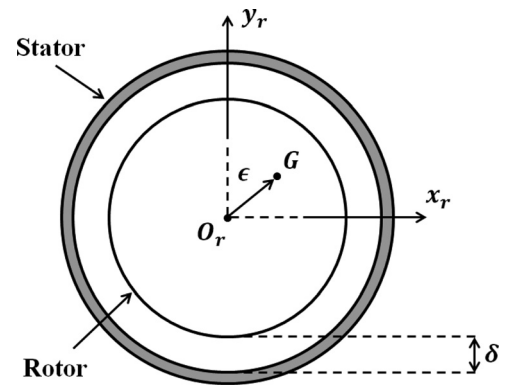

Fig. 3 Rotor–stator parameters (for clarity here, the viscoelastic stator supports are shown in Fig. 2)

proportional to the normal force by μ, and occurs in the negative relative tangential direction $\hat{e}_{\theta'}$. Thus, the contact forces are

$$\bar{F}_c = -k_c(r' - \delta)h(r' - \delta)\hat{e}_{r'} \tag{4}$$

$$\bar{F}_f = -\mu||\bar{F}_c||\hat{e}_{\theta'} \tag{5}$$

where the unit vector directions are

$$\hat{e}_{r'} = \cos\theta'\hat{i} + \sin\theta'\hat{j} \tag{6}$$

$$\hat{e}_{\theta'} = -\sin\theta'\hat{i} + \cos\theta'\hat{j} \tag{7}$$

and $h(r' - \delta)$ is the Heaviside function, representing the switch from noncontacting to contacting states of operation.

Observing Fig. 4, it is clear that $\cos\theta' = (u_{xr} - u_{xs})/r'$ and $\sin\theta' = (u_{yr} - u_{ys})/r'$. In this work, the range of considered shaft speeds is sufficiently high such that the friction force never reverses direction.

In reality, the viscoelastic suspension is an annular element; here, this radial component is accurately captured by its constitutive orthogonal components (as explained in Sec. 2.2). In essence, the viscoelastic suspension consists of a free spring k_0 in parallel with a fractional element. The fractional element is a spring k_1 in series with a fractional order springpot (η, α).

To properly account for the dynamics, a half degrees-of-freedom is imposed in the fractional element, between the spring and springpot for both the X and Y directions. Half degrees-of-freedom permit investigation of support elements (e.g., springs and dampers) mounted in series, and are distinguished from typical degrees-of-freedom by the lack of mass. Here, a subscript h will denote half degrees-of-freedom (e.g., u_{xh} and u_{yh}).

The mass of the rotor and stator are m_r and m_s, respectively. The rotor is supported on elastic bearings and a flexible shaft with stiffness coefficients k_b and k_s, respectively; the equivalent support stiffness of these flexible elements in series is k. Furthermore, the external viscous damping coefficient is c_b, which results in an equivalent damping ratio ζ. Referencing Fig. 3, the rotor's imbalance ϵ generates a force which occurs harmonically with the shaft rotation at frequency n. Balancing forces on the rotor, stator, and half degrees-of-freedom gives the system equations of motion, where the stator equations are

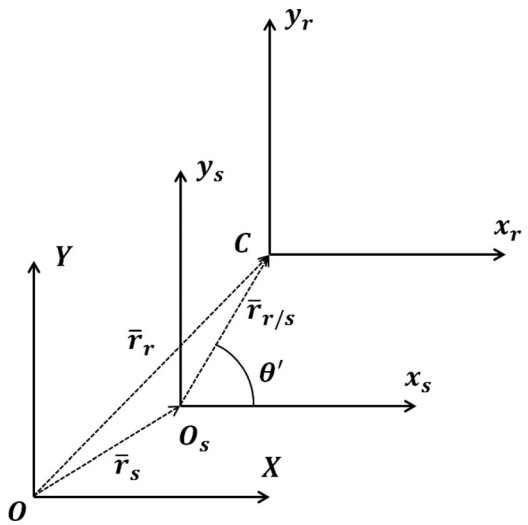

Fig. 4 Vector diagram showing the relationship between rotor and stator deflections

$$m_s\ddot{u}_{xs} - k_1u_{xh} + (k_0 + k_1)u_{xs} = k_c\frac{r' - \delta}{r'}\left[(u_{xr} - u_{xs}) - \mu(u_{yr} - u_{ys})\right] h(r' - \delta) \tag{8}$$

$$m_s\ddot{u}_{ys} - k_1u_{yh} + (k_0 + k_1)u_{ys} = k_c\frac{r' - \delta}{r'}\left[(u_{yr} - u_{ys}) + \mu(u_{xr} - u_{xs})\right] h(r' - \delta) - m_sg \tag{9}$$

A force balance on the half degrees-of-freedom yields

$$\eta\frac{d^\alpha u_{xh}}{dt^\alpha} + k_1u_{xh} - k_1u_{xs} = 0 \tag{10}$$

$$\eta\frac{d^\alpha u_{yh}}{dt^\alpha} + k_1u_{yh} - k_1u_{ys} = 0 \tag{11}$$

The superscript α denotes a fractional-derivate of order α, and is explained in greater detail in Sec. 2.2. Finally, the rotor equations of motion are

$$m_r\ddot{u}_{xr} + c\dot{u}_{xr} + ku_{xr} = k_c\frac{r' - \delta}{r'}\left[\mu(u_{yr} - u_{ys}) - (u_{xr} - u_{xs})\right] h(r' - \delta) + m_r\epsilon n^2\cos(nt) \tag{12}$$

$$m_r\ddot{u}_{yr} + c\dot{u}_{yr} + ku_{yr} = -k_c\frac{r' - \delta}{r'}\left[(u_{yr} - u_{ys}) + \mu(u_{xr} - u_{xs})\right] h(r' - \delta) - m_rg + m_r\epsilon n^2\sin(nt) \tag{13}$$

2.2 Viscoelasticity. Viscoelasticity describes a material that is time-dependent, or historic. This is in contrast to an elastic material, which is time-invariant. The historic nature of a viscoelastic material gives it unique properties in rotordynamic systems. A viscoelastic support is time, and correspondingly, frequency dependent. Therefore, the stiffness and damping properties vary depending on the operating conditions. If effectively harnessed, viscoelasticity can potentially reduce unwanted behavior in rotating systems, including wear from rotor–stator rub.

A large number of models exist for viscoelastic materials. For dynamic modeling, the most natural viscoelastic representations are those of spring and dashpot hierarchies. An infinite number of these systems can be created, but a common model is shown in Fig. 5(*a*). This model is known as the standard linear solid (SLS), and consists of a free spring in parallel with a Maxwell element. The Maxwell element consists of a spring and dashpot in series. The time dependency of the SLS is apparent with instantaneous displacements, the SLS acts elasticity, and with slowly progressing displacements, the SLS acts viscously. The spring and dashpot hierarchies can be directly incorporated in the dynamic models with inclusion of additional degrees-of-freedom. The translation from material properties (E_i, η_i) to dynamic properties (k_i, c_i) is straightforward and amounts to a bookkeeping operation. In theory, an infinite number of Maxwell elements can be placed in parallel to provide a wide spectrum of viscoelastic behavior [20]. The resulting Prony series is a simple, unambiguous model of viscoelasticity. The advantage of the Prony series is that the model constants (corresponding to the springs and dashpots) can be fit with a simple material test. By employing a relaxation test (i.e., fixing strain and tracking stress), the material constants can be fit via least squares

$$E(t) = \frac{\sigma(t)}{\epsilon_0} = E_0 + \sum_{n=1}^{\infty} E_n e^{-\lambda_n t} \tag{14}$$

where

$$\lambda_n = \frac{E_n}{\eta_n} \tag{15}$$

However, the additional terms $E_{2,\ldots,n}$, $\eta_{2,\ldots,n}$ add modeling complexity to dynamic simulations by expanding the eigenvalue problem. To reduce modeling complexity, fractional calculus models are often used [21–29]. Shown in Fig. 5(*b*), fractional calculus replaces the damper in the SLS with a "spring-pot." Mathematically, the spring-pot describes a hybrid spring and dashpot behavior

$$\sigma_P = \eta \frac{d^\alpha \epsilon_p}{dt^\alpha} \tag{16}$$

where η takes on the nonconventional units MPa $\cdot$ s^α The spring-pot is regulated by the parameter α, which interpolates between spring and dashpot behavior, giving the fractional model more robustness than the Prony model. The fractional model is

$$E(t) = E_0 + \sum_{n=1}^{\infty} E_n E_\alpha \left(-\frac{E_n}{\eta_n} t^{\alpha_n} \right) \tag{17}$$

where E_α is the Mittag–Leffler function [30]

$$E_\alpha(z) = \sum_{k=0}^{\infty} \frac{z^k}{\Gamma(\alpha k + 1)} \tag{18}$$

In Eq. (18), Γ in the gamma function: $\Gamma(x) = (x-1)!$. The fractional model typically requires fewer elements to characterize viscoelasticity. However, due to the Mittag–Leffler function, the fractional model is challenging to implement in the time-domain without modification (although numerical routines are available from Ref. [31] that allow for evaluation of the Mittag–Leffler function). A unique case of the fractional calculus model, when $\alpha = 1/2$, yields an unambiguous time-domain representation. This is known as the complementary error function fractional calculus model (CERF) [32]

$$E(t) = E_0 + \sum_{n=1}^{\infty} E_n e^{(\mu_n{}^2 t)} \text{erfc}\ (\mu_n \sqrt{t}) \tag{19}$$

where E_n and μ_n are material properties and $\mu_n = E_n/\eta_n$. In Eq. (19), the complementary error function (erfc) decays at a faster rate than the exponential increases, giving an overall relaxation behavior. The CERF model is thermodynamically permissible in general [32,33], and incorporates the flexibility of fractional calculus and the simplicity of integer-order derivative models. The CERF has proven robust in describing a number of materials from polymers to cartilage [34,35].

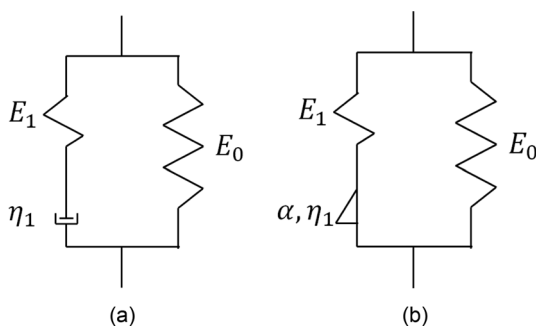

Fig. 5 Mechanical representation of viscoelastic models (*a*) SLS (prony series, $n = 1$) and (*b*) fractional model ($n = 1$)

The CERF model incorporates the advantages of fractional calculus (modeling flexibility) and integer-order viscoelasticity (unambiguous time-domain representation). In real materials, the coefficients $E_{0,\ldots,n}$ and $\mu_{1,\ldots,n}$ are determined from a simple stress-relaxation experiment. These stress/strain parameters are then translated to the desired dynamic quantities $k_{0,\ldots,n}$ and $c_{1,\ldots,n}$ in a manner similar to Refs. [36] and [37]. In the current study, the stress/strain parameters are directly translated to force/displacement parameters for simplicity in accessing the viscoelastic contribution to the rotor–stator dynamics. The remaining step is to integrate the CERF model into the dynamic simulation [33].

While the fractional calculus model provides advantages over other viscoelastic models, there are complications when incorporating fractional calculus in dynamic systems. In particular, the equations of motion and solution routine (i.e., MATLAB® ode45) rely on integer-order differential equations. Therefore, it is desired to make the fractional model compatible with such simulations. This is done by approximating the fractional derivative only in terms of integer-order derivatives. A numerical scheme is provided by Pooseh et al. [38] for the left Riemann–Liouville definition of a fractional derivative. By expanding the fractional derivative about the point a, and calculating the moments of the function, the approximation of a fractional derivative is made [38]

$$\begin{aligned} {}_aD_t^\alpha x(t) \approx\ & A(\alpha, N)(t-a)^{-\alpha} x(t) \\ & + B(\alpha, N)(t-a)^{1-\alpha} \dot{x}(t) \\ & - \sum_{p=2}^{N} C(\alpha, p)(t-a)^{1-p-\alpha} V_p(t) \end{aligned} \tag{20}$$

where

$$A(\alpha, N) = \frac{1}{\Gamma(1-\alpha)} \left[1 + \sum_{p=2}^{N} \frac{\Gamma(p-1+\alpha)}{\Gamma(\alpha)(p-1)!} \right] \tag{21}$$

$$B(\alpha, N) = \frac{1}{\Gamma(2-\alpha)} \left[1 + \sum_{p=1}^{N} \frac{\Gamma(p-1+\alpha)}{\Gamma(\alpha-1)p!} \right] \tag{22}$$

$$C(\alpha, p) = \frac{1}{\Gamma(2-\alpha)\Gamma(\alpha-1)} \frac{\Gamma(p-1+\alpha)}{(p-1)!} \tag{23}$$

and the moments, $V_p(t)$ for $p = 2,3,\ldots$, are found from the solution to the system of first-order differential equations

$$\begin{aligned} \dot{V}_p(t) &= (1-p)(t-a)^{p-2} x(t) \\ V_p(a) &= 0, \quad p = 2, 3, \ldots. \end{aligned} \tag{24}$$

In practice, N must be a computationally manageable number. The error in the approximation is not known a priori, therefore some calibration is needed to correctly access N based on the system dynamics. The advantage of the preceding routine is that a single initial condition, $x(t_0)$, is all that is needed to solve the fractional differential equation. This is paramount for numerical simulations of systems of differential equations.

The integer-order approximation is easily incorporated in a numerical solver like MATLAB's ODE45 without significant computational burden (depending on the value of N). Each of the first order differential equations from Eq. (24) for $p = 2,\ldots, N$ is incorporated in the state-space model alongside the equations of motion for the coupled system. The system is solved simultaneously at each increment in time.

The fractional calculus viscoelastic model represents a tradeoff in modeling complexity and simulation time. Using the fractional derivative $\alpha = 1/2$ allows for simple time-domain fitting of material properties, while retaining the flexibility of fractional calculus. The CERF is incorporated naturally into integer-order

differential equation solvers with the aforementioned approximation. The rotordynamic simulations including the viscoelastic stator support are given in Sec. 3.

3 Results

The equations of motion (Eqs. (8)–(13)) are integrated numerically using MATLAB's explicit hybrid fourth- and fifth-order variable-step Runge–Kutta solver, ode45. The integration tolerances are carefully selected due to small rotor–stator interferences; here, the relative and absolute tolerances are set to 10^{-9} and 10^{-13}, respectively. Appropriate tolerances are selected by progressively tightening the tolerance until convergence is obtained and the frequency spectrum shows no numeric noise. The rotor's static deflection is used as the initial condition in each case, with zero initial velocity; the system is then set into motion via the nonautonomous imbalance terms in the equations of motion. Only the rotor's steady-state response is considered. The parameters used in the example simulations are given in Table 1.

Example responses comparing the rigidly and flexibly mounted stators are shown in Figs. 6(*a*) and 6(*b*), respectively. In both cases, the response has been normalized by the clearance δ; Fig. 6(*a*) plots the fixed clearance for reference (a similar representation could be used in Fig. 6(*b*) by plotting the relative rotor deflection r' instead of the absolute deflections of both the rotor and stator, but such a display is further abstraction). It is clear upon comparing Figs. 6(*a*) and 6(*b*) that flexibly mounting the stator changes the rotor motion significantly. Effectively harnessing this motion could prevent damage in rotor–stator systems.

Contemporaneous points have been labeled in Fig. 6(*b*) to assist in understanding the relationship between the rotor and stator orbits. Prior to point 1 on the rotor orbit, the rotor is traveling upward; when the relative deflection r' exceeds the clearance δ, the rotor impacts the stator (shown as point 1 on the stator orbit). This impact perturbs the stator in the direction of the rotor motion, causing the stator to arc upward; it reaches its maximum, and begins to travel downward. At point 2, the rotor generates a second contact. At this second contact point, the stator velocity is sufficient to impart a significant downward velocity to the rotor. Qualitatively similar results are provided by Popprath and Ecker [39] for a stator suspended on a conventional spring-damper support, where chasing-type contemporaneous motions are shown for the rotor and stator.

The viscoelastically suspended rotor–stator system is capable of a rich variety of nonlinear responses, including periodic, quasiperiodic, and chaotic orbits (see Ref. [4] for a detailed description of these response types). An example periodic orbit is shown in Fig. 7(*a*) with its corresponding Poincaré section, where the rotor and stator contact four times per revolution (the Poincaré section is a stroboscopic sampling of the response, and is used to ascertain the qualitative nature of a particular response [4]). As expected, the frequency spectrum in Fig. 7(*b*) shows frequencies occurring at integer multiples of the shaft speed. At a different shaft speed ($n = 1.5\omega_n$, where $\omega_n = \sqrt{k/m_r}$, the rotor's natural frequency), the contact becomes quasiperiodic, as shown in Fig. 8(*a*) and identified by: (a) a closed-loop Poincaré section and (b) incommensurate frequencies in the frequency spectrum. A representative aperiodic (i.e., chaotic) response is shown in Fig. 9 for $n = 1.25\omega_n$, where no discernible pattern is visible in either the rotor or stator motion and the frequency content is generally broadband, but modulated by shaft speed harmonics.

These types of motions are typical of piecewise-smooth dynamical systems, and are observed in many rotor rub studies, both experimental and analytical (for example, see Refs. [4,5,7,40–42], among numerous others available in the literature). In addition to showing periodic, quasiperiodic, and chaotic responses, many other works have performed parametric studies using bifurcation analysis [5,6,43–46], focusing on parameters such as imbalance, rotor mass, friction coefficient, and clearance, among others. The parameters chosen in the current study are conducive to rich nonlinear behavior. A litany of configurations and properties exist in

Table 1 Simulation parameters used to generate orbits

Parameter	Symbol	Value (units)
Rotor mass	m_r	2 (kg)
Rotor external damping ratio	ζ	0.35
Equivalent support stiffness	k	$1 \cdot 10^6$ (N/m)
Contact stiffness	k_c	$10^4 \cdot k$
Eccentricity	ϵ	$0.4 \cdot 10^{-4}$ (m)
Clearance	δ	$0.8 \cdot 10^{-4}$ (m)
Friction coefficient	u	0.2
Stator mass	m_s	$3m_r$ (kg)
Free spring constant	k_0	$1 \cdot 10^6$ (N/m)
Viscoelastic spring constant	k_1	$1 \cdot 10^6$ (N/m)
Spring-pot constant	c_1	$1 \cdot 10^5$ (N $\cdot$ s$^{1/2}$)

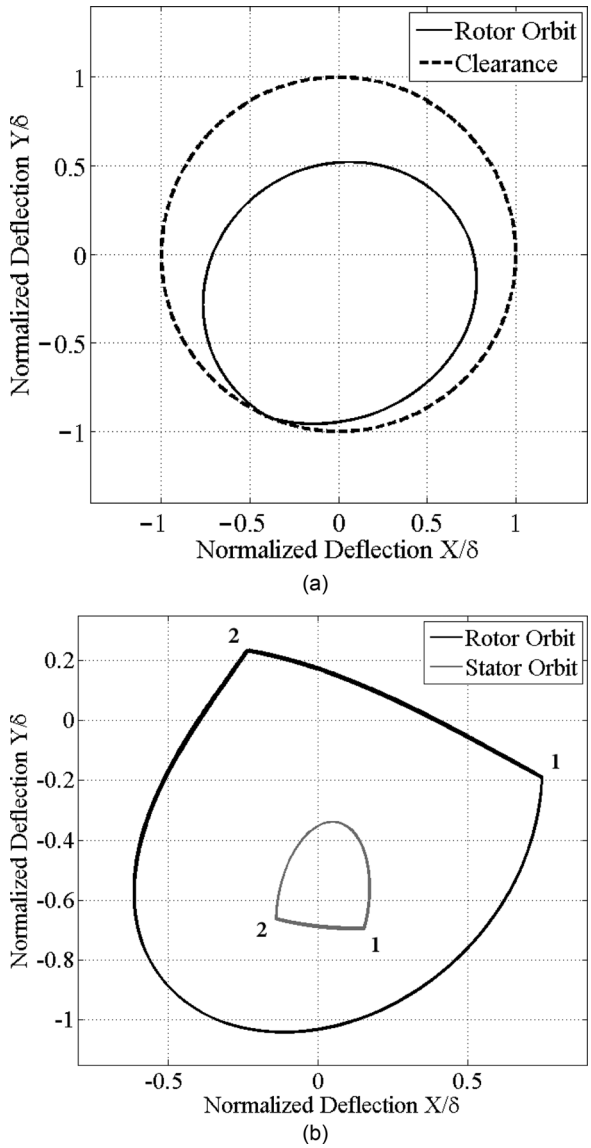

Fig. 6 Comparing the rigidly and flexibly mounted stators using parameters provided in Table 1 (responses calculated at $n/\omega_n = 1.1$). (*a*) Rigidly mounted stator, where the dashed circle represents the clearance and (*b*) flexibly mounted stator (for validation purposes, compare the response shown here to those provided by Popprath and Ecker [39]).

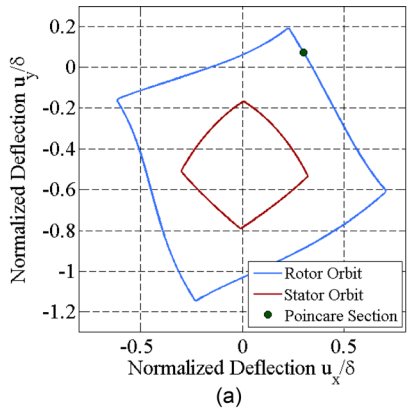

(a)

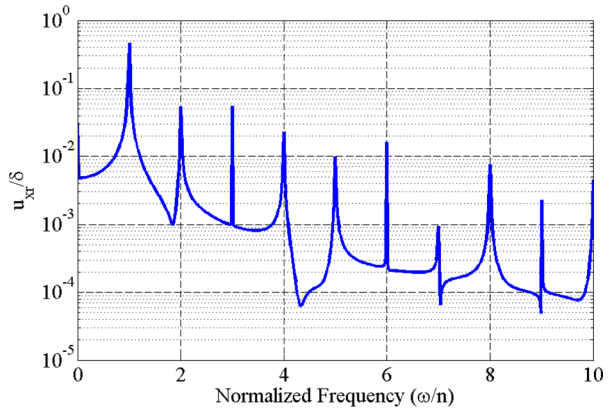

(b)

Fig. 7 Example periodic response for the viscoelastically suspended stator system ($n/\omega_n = 1.6$): (*a*) rotor and stator orbits and (*b*) rotor frequency spectrum

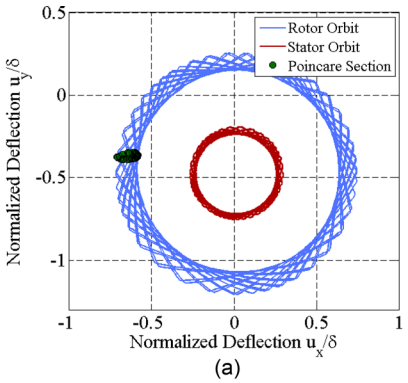

(a)

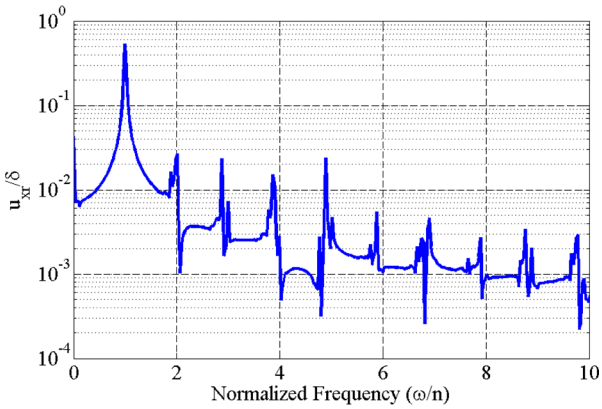

(b)

Fig. 8 Example quasiperiodic response for the viscoelastically suspended stator system ($n/\omega_n = 1.5$): (*a*) rotor and stator orbits and (*b*) rotor frequency spectrum

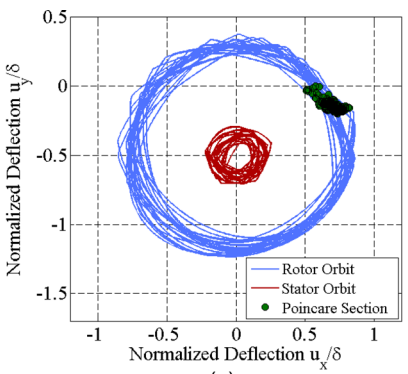

(a)

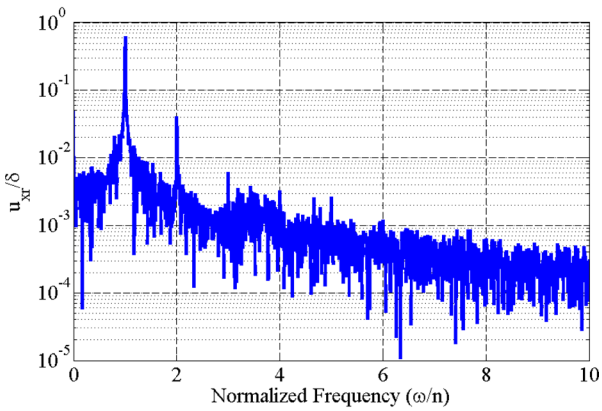

(b)

Fig. 9 Example chaotic response for the viscoelastically suspended stator system ($n/\omega_n = 1.25$): (*a*) rotor and stator orbits and (*b*) rotor frequency spectrum

real-world applications. Such specificity extends outside the scope of this work, where the purpose is to introduce tools and concepts useful for analyzing viscoelasticity in rotor–stator rub events. A similar parametric bifurcation study is left for future investigations based on specific application.

An adept tool for concisely summarizing the qualitative behavior of nonlinear systems is the bifurcation diagram, where one control parameter is varied and the resulting nature of the response is observed using the Poincaré section. A shaft speed bifurcation is performed on the rotor–stator system and shown in Fig. 10, where the qualitative nature of the response is ascertained using the magnitude of the rotor displacement. Prior to approximately $n/\omega_n = 0.85$, the rotor and stator are not in contact; once the rotor exceeds the allowable clearance, contact occurs and the rotor and stator motions persist in period-1 motion until approximately $n/\omega_n = 1.23$. At this point, the rotor motion experiences a grazing bifurcation [45] and transitions immediately into chaotic motion. This chaotic window exists for shaft speeds up to $n/\omega_n = 1.4$, where the response once again bifurcates, but this time into quasiperiodic motion. These results indicate that the rotor's response to contact is incredibly complex, and demonstrates rich variation in character as the system parameters are varied.

Importantly, this character of rich nonlinear behavior has been documented in the literature for similar systems (e.g., see Ref. [5] or [4]). Other analytic studies considering a flexibly suspended stator have also shown similar chasing motions, such as analytic simulations performed by Chang-Jian and Chen [42,47], who studied a stator suspended by a simple cubic spring support.

4 Discussion

Provided herein is a method for including viscoelasticity in a flexibly mounted stator that experiences rotor–stator rub. Two viscoelastic models are discussed, and the framework for

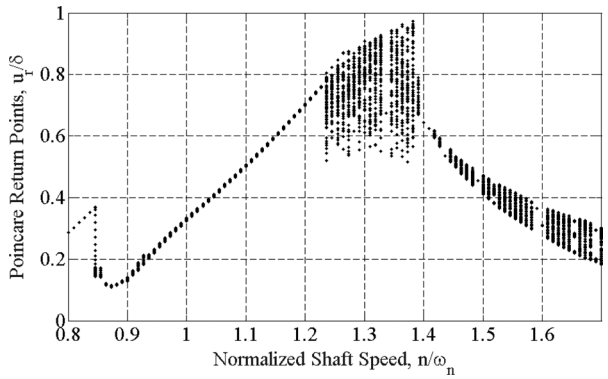

Fig. 10 Shaft speed bifurcation diagram showing numerous bifurcations and a generally rich nonlinear response

including viscoelasticity is provided. The SLS model is unambiguous and incorporates naturally in a dynamic system because it can be represented as a collection of springs and dashpots. However, if the SLS cannot be accurately fit to a real material, the CERF model may be employed. The CERF model is proposed as a hybrid model for viscoelastic behavior because it retains advantages of fractional and integer-order viscoelastic models. The CERF model is likewise easily fit in the time-domain, and incorporated in a dynamic system with the algorithm provided by Pooseh et al. [38]. It is proposed that if a flexibly mounted stator is used, realistically the support is viscoelastic in nature. Therefore, the SLS or CERF model can be used, depending on the material behavior.

The responses provided herein demonstrate the richness of the strongly nonlinear viscoelastically suspended rotor–stator system. Further analysis is needed to quantify such effects and the resulting contact forces and contact durations. The objective of the present work is to present a method for incorporating viscoelasticity into rotor–stator impact systems. Such a model is proposed as an important tool for understanding the nonlinear dynamics of complex systems. A comprehensive parametric analysis of shaft speed and viscoelasticity could perhaps be used to better understand the system behavior or design an optimum viscoelastic support, but such a study extends beyond the purview of this work.

5 Conclusion

The objective of modeling rotor–stator rub is to understand and ultimately reduce triboelement damage via real-time condition monitoring and improved component design. A necessary prerequisite for either of these tasks is robust and accurate system modeling. The coupled rotordynamic–viscoelastic model developed herein provides a method for analyzing rotordynamics when viscoelasticity is desired (specifically, this work investigated viscoelasticity in the support of a rotor–stator system). This framework and analysis tool could possibly be used for further analysis of rotor–stator rub systems, where it is hypothesized that contact alone is not the detriment of triboelements, but rather impulsive forces from contact. Once a specific system and viscoelastic material is selected for analysis, the contact duration and impulsive loading could be quickly determined to ascertain the advantages and disadvantages of such a support arrangement.

Nomenclature

c = rotor damping coefficient
c_b = external bearing damping coefficient
E_α = Mittag–Leffler function
$E(t)$ = viscoelastic relaxation modulus
$\bar{F}_C$ = normal contact force
$\bar{F}_f$ = frictional force
g = acceleration due to gravity
k = equivalent rotor support stiffness
k_b = external bearing stiffness
k_c = rotor–stator contact stiffness
k_s = rotor shaft stiffness
k_0 = free spring stiffness
k_1 = fractional element stiffness
m_r = rotor mass
m_s = stator mass
n = shaft speed
r' = relative rotor–stator clearance
u_{xh}, u_{yh} = half degrees-of-freedom deflections
u_{xr}, u_{yr} = rotor deflection in x and y directions
u_{xs}, u_{ys} = stator deflection in x and y directions
α = fractional derivative parameter
Γ = gamma function
δ = set-point rotor–stator clearance
ϵ = rotor eccentricity
ζ = viscous damping ratio
η = viscous/viscoelastic term constant
μ = dry friction coefficient

References

[1] Lee, A. S., and Green, I., 1994, "Higher Harmonic Oscillations in a Non-Contacting FMR Mechanical Face Seal Test Rig," ASME J. Vib. Acoust., **116**(2), pp. 161–167.
[2] Bernardo, M., Budd, C., Champneys, A. R., and Kowalczyk, P., 2008, *Piecewise-Smooth Dynamical Systems: Theory and Applications*, Springer Science and Business Media, Springer-Verlag, London.
[3] Varney, P., and Green, I., 2014, "Rotor/Stator Rubbing Contact in an Overhung Rotordynamic System," STLE Annual Meeting, Orlando, FL.
[4] Varney, P., and Green, I., 2014, "Nonlinear Phenomena, Bifurcations, and Routes to Chaos in an Asymmetrically Supported Rotor-Stator Contact System," J. Sound Vib., **336**, pp. 207–226.
[5] Chu, F., and Zhang, Z., 1997, "Bifurcation and Chaos in a Rub-Impact Jeffcott Rotor System," J. Sound Vib., **210**(1), pp. 1–18.
[6] Zhang, W. M., and Meng, G., 2006, "Stability, Bifurcation and Chaos of a High-Speed Rub-Impact Rotor System in Mems," Sens. Actuators, **127**(1), pp. 163–178.
[7] Groll, G. V., and Ewins, D. J., 2002, "A Mechanism of Low Subharmonic Response in Rotor/Stator Contact Measurements and Simulation," ASME J. Vib. Acoust., **124**(3), pp. 350–358.
[8] Jacquet-Richardet, G., Torkhani, M., Cartraud, P., Thouverez, F., Baranger, T. N., Herran, M., Gibert, C., Baguet, S., Almeida, P., and Peletan, L., 2013, "Rotor to Stator Contacts in Turbomachines Review and Application," Mech. Syst. Signal Process., **40**(2), pp. 401–420.
[9] Yu, J. J., Goldman, P., Bently, D. E., and Muzynska, A., 2002, "Rotor/Seal Experimental and Analytical Study on Full Annular Rub," ASME J. Eng. Gas Turbines Power, **124**(2), pp. 340–350.
[10] Childs, D. W., and Bhattacharya, A., 2007, "Prediction of Dry-Friction Whirl and Whip Between a Rotor and a Stator," ASME J. Vib. Acoust., **129**(3), pp. 355–362.
[11] Yu, J., 2012, "On Occurrence of Reverse Full Annular Rub," ASME J. Eng. Gas Turbines Power, **134**(1), pp. 219–227.
[12] Cao, J., Ma, C., Jiang, Z., and Liu, S., 2011, "Nonlinear Dynamic Analysis of Fractional Order Rub-Impact Rotor System," Commun. Nonlinear Sci. Numer. Simul., **16**(3), pp. 1443–1463.
[13] Patel, T. H., Zuo, M. J., and Zhao, X., 2012, "Nonlinear Lateral-Torsional Coupled Motion of a Rotor Contacting a Viscoelastically Suspended Stator," Nonlinear Dyn., **69**(1), pp. 325–339.
[14] Dutt, J. K., and Nakra, B. C., 1992, "Stability of Rotor Systems With Viscoelastic Supports," J. Sound Vib., **153**(1), pp. 89–96.
[15] Lee, Y. B., Kim, T. H., Lee, N. S., and Choi, D. H., 2004, "Dynamic Characteristics of a Flexible Rotor System Supported by a Viscoelastic Foil Bearing (VEFB)," Tribol. Int., **37**(9), pp. 679–687.
[16] Shabaneh, N. H., and Zu, J. W., 2000, "Dynamic Analysis of Rotor-Shaft Systems With Viscoelastically Supported Bearings," Mech. Mach. Theory, **35**(9), pp. 1313–1330.
[17] Wilkes, J., Moore, J., Ransom, D., and Vannini, G., 2014, "An Improved Catcher Bearing Model and an Explanation of the Forward Whirl/Whip Phenomenon Observed in Active Magnetic Bearing Transient Drop Experiments," ASME J. Eng. Gas Turbines Power, **136**(4), pp. 1–11.
[18] Sun, G., Palazzolo, A., Provenza, A., and Montague, G., 2004, "Detailed Ball Bearing Model for Magnetic Suspension Auxiliary Service," J. Sound Vib., **269**(3–5), pp. 933–963.
[19] Beatty, R. F., 1985, "Differentiating Rotor Response Due to Radial Rubbing," J. Vib., Acoust., Stress, Reliab. Des., **107**(2), pp. 151–160.
[20] Smyth, P. A., Green, I., Jackson, R. L., and Hanson, R. R., 2014, "Biomimetic Model of Articular Cartilage Based on In Vitro Experiments," J. Biomimetics, Biomater. Biomed. Eng., **21**, pp. 75–91.
[21] Bagley, R. L., and Torvik, P. J., 1979, "A Generalized Derivative Model for an Elastomer Damper," Shock Vib. Bull., **49**(2), pp. 135–143.

[22] Bagley, R. L., and Torvik, P. J., 1983, "A Theoretical Basis for the Application of Fractional Calculus to Viscoelasticity," J. Rheol. (1978-Present), **27**(3), pp. 201–210.
[23] Rogers, L., 1983, "Operators and Fractional Derivatives for Viscoelastic Constitutive Equations," J. Rheol., **27**(4), pp. 351–372.
[24] Koeller, R., 1984, "Applications of Fractional Calculus to the Theory of Viscoelasticity," ASME J. Appl. Mech., **51**(2), pp. 299–307.
[25] Torvik, P. J., and Bagley, R. L., 1984, "On the Appearance of the Fractional Derivative in the Behavior of Real Materials," ASME J. Appl. Mech., **51**(2), pp. 294–298.
[26] Bagley, R. L., and Torvik, P. J., 1985, "Fractional Calculus in the Transient Analysis of Viscoelastically Damped Structures," AIAA J., **23**(6), pp. 918–925.
[27] Bagley, R. L., and Torvik, P. J., 1986, "On the Fractional Calculus Model of Viscoelastic Behavior," J. Rheol. (1978-Present), **30**(1), pp. 133–155.
[28] Koeller, R. C., 1986, "Polynomial Operators, Stieltjes Convolution, and Fractional Calculus in Hereditary Mechanics," Acta Mech., **58**(3–4), pp. 251–264.
[29] Bagley, R. L., 1989, "Power Law and Fractional Calculus Model of Viscoelasticity," AIAA J., **27**(10), pp. 1412–1417.
[30] Erdelyi, A., Magnus, W., Oberhettinger, F., and Tricomi, F., eds., 1955, *Higher Transcendental Functions*, Vol. III, McGraw-Hill, New York.
[31] Podlubny, I., 1998, *Fractional Differential Equations: An Introduction to Fractional Derivatives, Fractional Differential Equations, to Methods of Their Solution and Some of Their Applications, Mathematics in Science and Engineering*, Academic Press, San Diego, CA.
[32] Szumski, R. G., and Green, I., 1991, "Constitutive Laws in Time and Frequency Domains for Linear Viscoelastic Materials," J. Acoust. Soc. Am., **90**(40), p. 2292.
[33] Szumski, R. G., 1993, "A Finite Element Formulation for the Time Domain Vibration Analysis of an Elastic-Viscoelastic Structure," Ph.D. thesis, Georgia Institute of Technology, Atlanta, GA.
[34] Biesel, V., 1993, "Experimental Measurement of the Dynamic Properties of Viscoelastic Materials," M.S. thesis, Georgia Institute of Technology, Atlanta, GA.
[35] Smyth, P. A., and Green, I., 2015, "A Fractional Calculus Model of Articular Cartilage Based on Experimental Stress-Relaxation," Mech. Time-Depend. Mater., **19**(2), pp. 209–228.
[36] Scholz, A., 2011, "Ein beitrag zur optimierung des schwingungsverhaltens komplexer rotorsysteme mit viskoelastischen dämpfungselementen," Ph.D. thesis, Technische Universitat Berlin, Berlin.
[37] Liebich, R., Scholz, A., and Wieschalla, M., 2012, "Rotors Supported by Elastomer-Ring-Dampers: Experimental and Numerical Investigations," 10th International Conference on Vibrations in Rotating Machinery, London, pp. 443–453.
[38] Pooseh, S., Almeida, R., and Torres, D. F. M., 2013, "Numerical Approximations of Fractional Derivatives With Applications," Asian J. Control, **15**(3), pp. 698–712.
[39] Popprath, S., and Ecker, H., 2007, "Nonlinear Dynamics of a Rotor Contacting an Elastically Suspended Stator," J. Sound Vib., **308**(3–5), pp. 767–784.
[40] Chu, F., and Zhang, Z., 1997, "Periodic, Quasi-Periodic and Chaotic Vibrations of a Rub-Impact Rotor System Supported on Oil Film Bearings," Int. J. Eng. Sci., **35**(9), pp. 963–973.
[41] Goldman, P., and Muszynska, A., 1994, "Dynamic Effects in Mechanical Structures With Gaps and Impacting: Order and Chaos," ASME J. Vib. Acoust., **116**(4), pp. 541–547.
[42] Chang-Jian, C. W., and Chen, C. K., 2007, "Chaos and Bifurcation of a Flexible Rub-Impact Rotor Supported by Oil Film Bearings With Nonlinear Suspension," Mech. Mach. Theory, **42**(3), pp. 312–333.
[43] Kim, Y. B., and Noah, S. T., 1990, "Bifurcation Analysis for a Modified Jeffcott Rotor With Bearing Clearances," Nonlinear Dyn., **1**(3), pp. 221–241.
[44] Inayat-Hussain, J. I., 2010, "Bifurcations in the Response of a Jeffcott Rotor With Rotor-to-Stator Rub," ASME Paper No. ESDA2010-24453.
[45] Chavez, J. P., and Wiercigroch, M., 2013, "Bifurcation Analysis of Periodic Orbits of a Non-Smooth Jeffcott Rotor Model," Commun. Nonlinear Sci. Numer. Simul., **18**(9), pp. 2571–2580.
[46] Abu-Mahfouz, I., and Banerjee, A., 2013, "On the Investigation of Nonlinear Dynamics of a Rotor With Rub-Impact Using Numerical Analysis and Evolutionary Algorithms," Proc. Comput. Sci., **20**, pp. 140–147.
[47] Chang-Jian, C. W., and Chen, C. K., 2009, "Chaos of Rub-Impact Rotor Supported by Bearings With Nonlinear Suspension," Tribol. Int., **42**(3), pp. 426–439.